Appl Phys A (2009) 95: 573–578
DOI 10.1007/s00339-008-4953-9

Applied Physics A
Materials Science & Processing

Solidification velocity in liquid silicon during excimer laser crystallization

Chil-Chyuan Kuo

Received: 8 April 2008 / Accepted: 7 July 2008 / Published online: 15 November 2008
© Springer-Verlag 2008

Abstract Excimer laser crystallization (ELC) is commonly employed to fabricate low-temperature polycrystalline silicon. A time-resolved in-situ optical system with nanosecond response time is developed to monitor and record the phase transformation process during ELC. The average solidification velocity of liquid silicon (liquid Si) is investigated from the optical spectra recorded by a fast oscilloscope. It is found that the average solidification velocities of liquid Si in the partial-melting and complete-melting regimes are fundamentally different. In the partial-melting regime, the average solidification velocity decreases with increasing excimer laser energy density; while in the complete-melting regime, it increases abruptly due to the presence of deeply supercooled liquid Si.

PACS 68.55 · 78.30 · 81.40

1 Introduction

Excimer laser crystallization (ELC) is an efficient technology for fabricating high-performance low-temperature polycrystalline silicon (poly-Si) thin-film transistors (TFTs) for advanced flat panel display application such as super-high-definition active matrix liquid crystal displays (AMLCDs) and active matrix organic light-emitting diode displays (AMOLEDs) since poly-Si films are the key material of TFTs [1, 2]. The major advantage of the poly-Si TFTs for AMLCDs and AMOLEDs is the increase in carrier mobility and the ability to integrate the pixel switching elements and peripheral driving circuit on the same substrate [3].

The solid phase of Si thin films is semiconducting, while their liquid phase is metallic [4]. Hence, their physical properties such as optical, electrical, and thermal constants for the liquid and solid phases are significantly different even at similar temperature and pressure. Such differences in physical properties provide unique opportunities for in-situ real-time optical measurements of the phase transformation of Si thin films. Time-resolved optical reflectivity and transmissivity measurements are most commonly employed to investigate the rapid melting and solidification scenarios in semiconductors [5]. The solidification velocity of liquid silicon (liquid Si) is a critical parameter in the fabrication of high-performance low-temperature polycrystalline silicon thin-film transistors (LTPS TFTs) because lowering the solidification velocity of liquid Si results in delaying the time for nucleation [6]. However, the solidification velocity of liquid Si during ELC is still not well understood, even though the ELC of silicon thin films have been thoroughly investigated for the past several years [7, 8].

In this work, a time-resolved in-situ optical reflection and transmission (TRORT) monitoring system, which comprises a probe laser, a digital oscilloscope, and two photodiodes, is developed to investigate the microstructural evolution of poly-Si films during ELC. After ELC, the optical spectra recorded by a fast oscilloscope are analyzed by MATLAB and EXCEL software. The average solidification velocities of liquid Si as functions of excimer laser energy density are investigated. Differences in the solidification velocity between the partial-melting and complete-melting regimes are discussed. Microstructural analyses of the resulting poly-Si films after ELC are performed using field emission scanning electron microscopy (FE-SEM).

C.-C. Kuo (✉)
Department of Mechanical Engineering,
Ming Chi University of Technology, No. 84, Gungjuan Road,
Taishan Taipei Hsien 243, Taiwan
e-mail: jacksonk@mail.mcut.edu.tw
Fax: +886-2-29063269

2 Experimental setup

Figure 1 shows a schematic illustration of sample structure and experimental setup for measuring reflectivity and transmissivity during ELC. Details of the experimental setup can be found elsewhere [9, 10]. Silane-based 90-nm-thick a-Si film is deposited on a 0.7-mm-thick Corning 1737 glass substrate covered with a 300-nm-thick SiO_2 layer by plasma-enhanced chemical vapor deposition (PECVD). In order to prevent the ablation caused by sudden hydrogen eruption during ELC, the samples are dehydrogenated by performing a thermal treatment at 500°C for 2 hours to reduce the hydrogen content [11]. The samples are held in self-closing tweezers at the end of a cantilever beam fixed on a motorized x–y linear translation stage (resolution = 0.625 μm). The movement of the focusing lens (focus = 100 mm) fixed on a motorized z-axis linear translation stage is precisely controlled to adjust the desired excimer laser energy density for crystallization. To enhance the efficiency of ELC, the movement of the three-axis (X–Y–Z) motorized translation stages can accurately be manipulated using the man–machine interface. A Joule meter is employed to calibrate the output energy of excimer laser pulse before ELC. The ELC experiments and measurements are performed at ambient environmental conditions of 300 K and below 60% relative humidity. The a-Si thin films are crystallized by a single-shot XeF excimer laser operating at 351 nm with 25-ns pulse duration, while the pulse-to-pulse energy fluctuations are less than ±10%. A stainless steel slit mask of around 2×15 mm^2 is employed to transform the incident Gaussian beam into a rectangular beam spot. A quartz beam splitter is employed to reflect 10% of the excimer laser beam to a photodetector for triggering a fast digital storage oscilloscope with a sample rate of 2 GHz/s. The size of the beam spot can be manipulated by changing the working distance between the focusing lens (cylindrical lens, $f = 100$ mm) and the sample surface. The transient phase transformation scenarios are monitored and recorded by measuring the time-resolved transmissivity and reflectivity using the TRORT monitoring system. An aperture with a diameter of 0.3 mm is mounted in front of the He–Ne probe laser to increase the resolution of TRORT measurements. The He–Ne probe laser is incident at 45° with respect to the normal to the sample's surface and focused on the center of the laser-irradiated spot. The reflected beam from the sample is focused on a fast photodiode (response time = 1 ns). An interference filter is mounted in front of the photodiode, allowing only red light from the He–Ne probe laser to contribute to the detected signal. Two photodetectors are positioned optimally to get the maximum signal before optical measurements. Following ELC, the optical spectra are analyzed by both MATLAB and EXCEL software. The average solidification velocities of liquid Si as functions of excimer laser energy density are also investigated by both MATLAB and EXCEL software. Microstructural analyses of the annealed poly-Si films after ELC are performed using FE-SEM operated at acceleration electron beam energy of 15 keV. Before FE-SEM observation, the crystallized silicon films are treated by Secco-etching to delineate the grain boundaries (GBs) and intragrain defects [12].

3 Results and discussion

Figure 2 shows the variations of the optical spectra measured by the TRORT monitoring system as functions of time for various excimer laser energy densities. Details of the phase transformation of Si thin films can be found elsewhere [13]. Melting and crystallization behavior of Si thin films can be extracted from the transient optical measurements [14]. Figure 3 shows a sample of optical spectra of

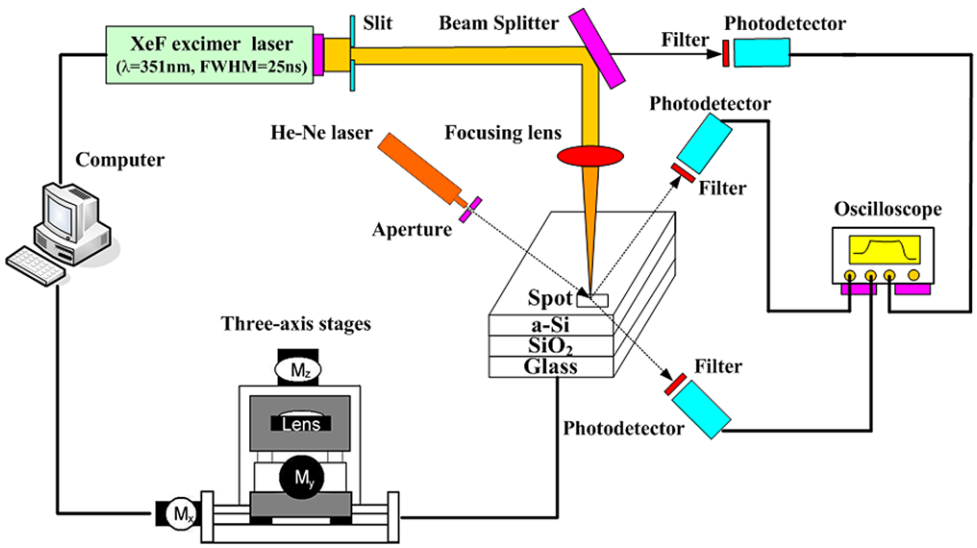

Fig. 1 Schematic illustration of the sample structure and experimental setup for measuring reflectivity and transmissivity during ELC

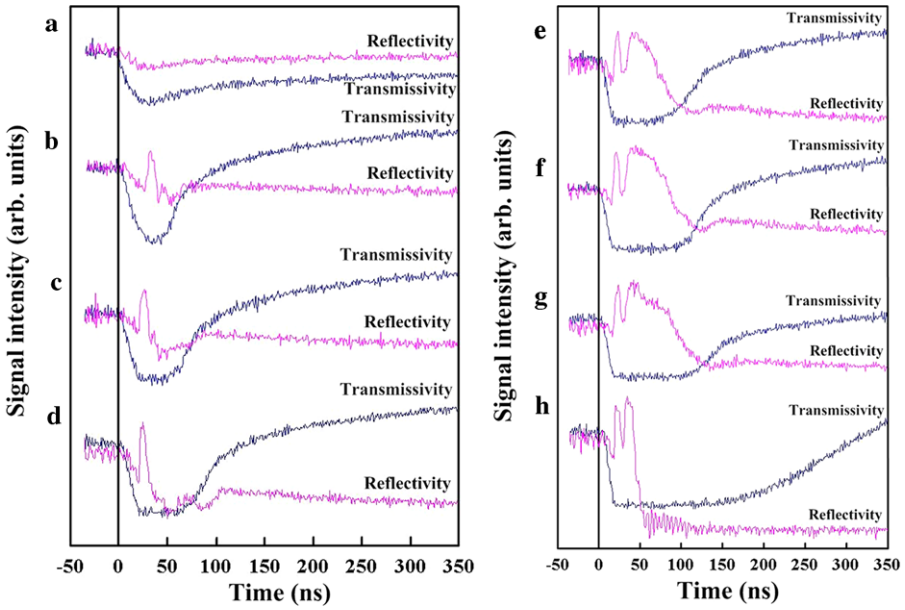

Fig. 2 Variations of the optical spectra measured by the TRORT monitoring system as functions of time for various excimer laser energy densities. Excimer laser energy density for **a**, **b**, **c**, **d**, **e**, **f**, **g**, and **h** is 75, 100, 130, 150, 175, 190, 200, and 225 mJ/cm^2, respectively

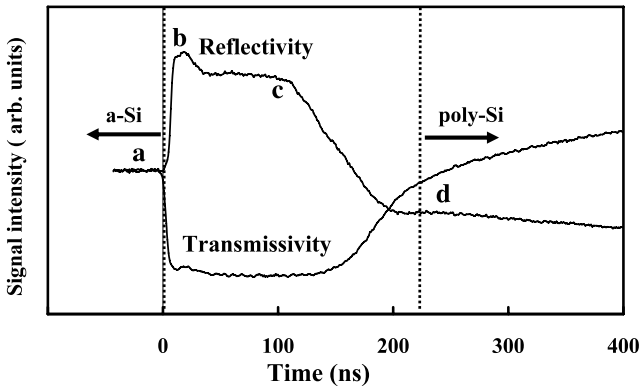

Fig. 3 A sample of optical spectra of reflectivity and transmissivity, indicating the melting and recrystallization evolution during ELC. The drastic drop in transmissivity and an abrupt rise in reflectivity correspond to the melting of Si thin films

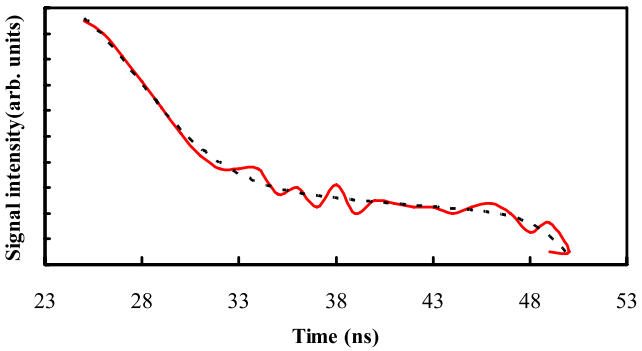

Fig. 4 Result of curve fitting by second-order polynomial fit. *Solid line* and *dashed line* represent the raw data of the spectra and the fitting curve, respectively

reflectivity and transmissivity, showing the melting and recrystallization evolution during ELC. The data are normalized to the initial reflectivity and transmissivity of a-Si thin films. The sample initially absorbs the excimer laser fluence (points a to b) and then melts. The reflection signal rises because the reflectivity of Si thin films changes from 32 to 76% upon melting during the phase transition from solid to liquid, which exhibits the metallic character [15]. The drastic drop in the transmission signal is caused by the crystallization of the liquid Si. A plateau (points b to c) in the reflectivity is observed because the melt depth of liquid Si is more than double the penetration depth of He–Ne probe laser [16]. Between points c and d, the reflectivity decreases, revealing the nucleation and solidification process [17]. Optical microscopy observation shows that the excimer laser fluence was sufficient to complete the melting of Si thin films. This is confirmed by the observation using FE-SEM.

With reference to the optical spectra recorded by a fast oscilloscope, the solidification velocity of liquid Si is analyzed by both MATLAB and EXCEL software. Figure 4 shows the result of curve fitting by second-order polynomial fit. The solid line and dashed line represent the raw data of the spectra and the fitting curve, respectively. As can be seen, the fitting curve is not consistent with the raw data of the spectra with the R^2 value being 0.9818 only. In order to enhance the accuracy of the fitting curve, sixth-order polynomial fit is employed for curve fitting applications. As seen in Fig. 5, the R^2 value is enhanced to 0.9874. Table 1 shows the results of the R^2 value and polynomial equation using polynomial fit of different orders. In general, the larger the R^2 value, the better the accuracy of the fitting curve is. In principle, high-order polynomial fit (>sixth-order polynomial fit) is suggested for analyzing the complicated or highly

Table 1 Results of the R^2 value and curve equation using different order of polynomial fit

Approach	R^2	Polynomial equation
Second-order polynomial	0.9317	$9 \times 10^{-6}x^2 - 8 \times 10^{-4}x + 0.0204$
Third-order polynomial	0.9819	$-8 \times 10^{-7}x^3 + 1 \times 10^{-4}x^2 - 4.1 \times 10^{-3}x + 0.0599$
Fourth-order polynomial	0.9841	$-3 \times 10^{-8}x^4 + 3 \times 10^{-6}x^3 - 1 \times 10^{-4}x^2 + 1.1 \times 10^{-3}x + 0.0136$
Fifth-order polynomial	0.9843	$1 \times 10^{-9}x^5 - 3 \times 10^{-7}x^4 + 2 \times 10^{-5}x^3 - 8 \times 10^{-4}x^2 + 1.1 \times 10^{-2}x - 0.073$
Sixth-order polynomial	0.9874	$-6 \times 10^{-10}x^6 + 1 \times 10^{-7}x^5 - 1 \times 10^{-5}x^4 + 6 \times 10^{-4}x^3 - 1.79 \times 10^{-2}x^2 + 2.594 \times 10^{-1}x - 1.5306$

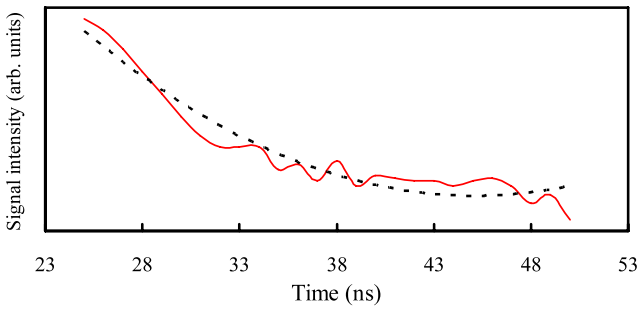

Fig. 5 Result of curve fitting by sixth-order polynomial fit. *Solid line* and *dashed line* represent the raw data of the spectra and the fitting curve, respectively

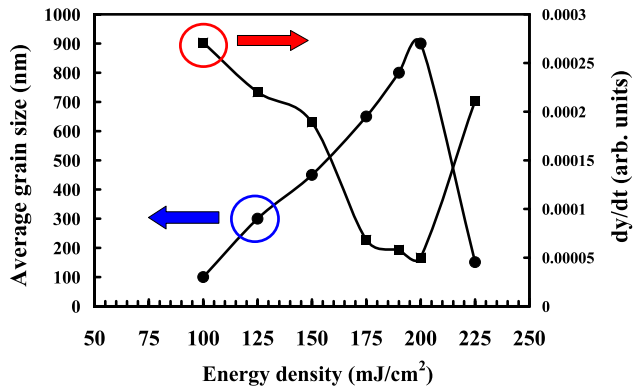

Fig. 6 Average grain size and dy/dt as functions of laser energy density. *Solid circles* and *solid squares* represent the data of average grain size and dy/dt, respectively

fluctuated data. Thus, a sixth-order polynomial fit is a good candidate for analyzing the solidification velocity of liquid Si in this work.

Figure 6 shows the average grain size and dy/dt as functions of laser energy density. The dy/dt stands for the slope of the fitting curve. As can be seen, the slope of the fitting curve decreases with increasing excimer laser energy density ($100\ \text{mJ/cm}^2 \leq E \leq 200\ \text{mJ/cm}^2$) and increases at higher excimer laser energy density ($200\ \text{mJ/cm}^2 < E \leq 225\ \text{mJ/cm}^2$). Boneberg and Leiderer showed that dy/dt is considered to be proportional to the solidification velocity in terms of the linear change of the reflectivity as a function of the phase transformation from liquid to solid state [16]. In general, the slower the solidification rate is, the larger the average grain size of poly-Si is [18]. Thus, the average grain size of poly-Si films will increase with increasing excimer laser energy density ($100\ \text{mJ/cm}^2 \leq E \leq 200\ \text{mJ/cm}^2$) and will decrease at higher excimer laser energy density ($200\ \text{mJ/cm}^2 < E \leq 225\ \text{mJ/cm}^2$). These results are confirmed by the observation using FE-SEM measurements, as shown in Fig. 7. In fact, the average grain size of poly-Si films increase with increasing excimer laser energy density ($100\ \text{mJ/cm}^2 \leq E \leq 200\ \text{mJ/cm}^2$) and decrease at higher excimer laser energy density ($200\ \text{mJ/cm}^2 < E \leq 225\ \text{mJ/cm}^2$). As shown in this figure, the average grain size is in the range of 100–900 nm, and the grains are generally elliptical in shape. In particular, a disk-shaped grain [19] with a diameter of approximately 1 μm is observed in the poly-Si films crystallized at excimer energy density of $215\ \text{mJ/cm}^2$. The disk-shaped grain is a single grain with low density of ingrain defects [20, 21]. The size of the fine grains surrounding the disk-shaped grain is approximately 50–100 nm in diameter. This finding is similar to the observations made by Mariucci et al. [22]. As expected, two distinct regrowth regimes (low excimer laser energy density and high excimer laser energy density) can clearly be observed [23, 24]. In the low excimer laser energy density regime ($100\ \text{mJ/cm}^2 \leq E \leq 200\ \text{mJ/cm}^2$), the average grain size of poly-Si films increases slowly because the melt depth increases with increasing excimer laser energy density. On the other hand, the average grain size of poly-Si films decreases abruptly in the high excimer laser fluence regime ($200\ \text{mJ/cm}^2 < E \leq 225\ \text{mJ/cm}^2$) because the recrystallization mechanism of Si thin films is changed [25], leading to

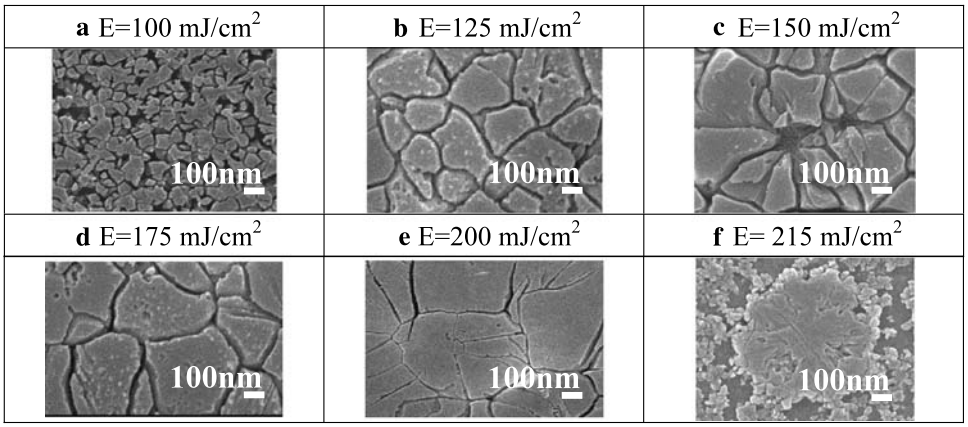

Fig. 7 FE-SEM micrograph of Secco-etched poly-Si films irradiated at different excimer laser energy densities

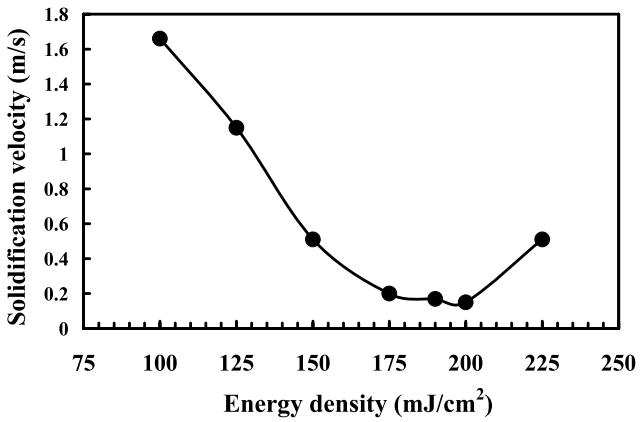

Fig. 8 Solidification velocity as a function of laser energy density

the reduction in average grain size of poly-Si films. These results are confirmed by the solidification velocity of liquid Si, as shown in Fig. 8. As can be seen, the solidification velocity of liquid-Si is not constant for various excimer laser energy densities. The solidification velocity of liquid Si at excimer laser energy density of 100 and 200 mJ/cm^2 are estimated to be 1.66 and 0.15 m/s, respectively. However, Gupta et al. [26] showed that the sufficiently high solidification velocity on the order of 10 m/s can be reached by numerical simulation using heat flow calculations. Obviously, the solidification velocity in this work is smaller than 10 m/s. Such differences can be attributed to the different thickness of Si thin films and the wavelength of excimer laser in both works. It should be pointed out that the solidification velocity of liquid-Si at excimer laser energy density of 225 mJ/cm^2 is estimated to be 0.51 m/s, resulting in a small grain structure because the homogeneous nucleation is triggered by deep supercooling during solidification [23]. This phenomenon is significantly supported by the classical nucleation theory [27], indicating that the critical grain size of poly-Si films decreases with increase in supercooling of liquid Si. This implies that the crystallization mechanisms of Si thin films are strongly dependent on the solidification velocity of liquid Si. Consequently, a tight control of the excimer laser energy density regarding a narrow processing window [28] during ELC is essential in the fabrication of advanced flat panel display such as AMOLEDs using LTPS TFTs. Some major problems in the ELC process, such as surface roughness and uniformity of poly-Si films for mass production of LTPS TFTs, still remain to be investigated. Furthermore, fabrication of high-performance LTPS TFTs with very few GBs perpendicular to the current flow by controlling the grain alignment in the poly-Si active layer is required.

4 Conclusion

A time-resolved in-situ optical system with nanosecond response time has been developed to monitor and record the crystallization kinetics of Si thin films during ELC. The average solidification velocity of liquid Si has been investigated from the spectra recorded by optical measurements. Experimental results suggest that the solidification velocity of liquid Si plays an important role in the recrystallization process of Si thin films. The average solidification velocities of liquid Si in the partial-melting and complete-melting regimes are significantly different. In the partial-melting regime, the average solidification velocity decreases with increasing excimer laser energy density, while it increases abruptly in the complete-melting regime due to the presence of deeply supercooled liquid Si. The results reported here showed great advantage for the realization of high-performance LTPS TFTs on a large-area glass substrate under the optimum experimental conditions by ELC.

Acknowledgements This work was financially supported by the National Science Council of Taiwan under Contract No. NSC 96-2221-E-131-003. The author would like to thank Professors W.C. Yeh and J.Y. Jeng of the National Taiwan University of Science and Technology for assistance with related experimental apparatus. The skillful technical assistance of Mr. C.P. Hsiao of the National Taiwan University of Science and Technology and Mr. J.Y. Lin of the Ming Chi University of Technology are highly appreciated.

References

1. G.K. Giust, T.W. Sigmon, IEEE Trans. Electron. Devices **47**, 207 (2000)
2. K. Nakazawa, J. Appl. Phys. **69**, 1703 (1991)
3. Y.F. Chong, K.L. Pey, A.T.S. Wee, M.O. Thompson, C.H. Tung, A. See, Appl. Phys. Lett. **81**, 3786 (2002)
4. G.E. Jellison, D.H. Lowndes, Appl. Phys. Lett. **47**, 718 (1985)
5. M. Hatano, S. Moon, M. Lee, K. Suzuki, C.P. Grigoropoulos, J. Non-Cryst. Solids **266**, 654 (2000)
6. H. Kuriyama, S. Kiyama, S. Noguchi, T. Kuwahara, S. Ishida, T. Nohda, K. Sano, H. Iwata, H. Kawata, M. Osumi, S. Tsuda, S. Nakano, Y. Kuwano, Jpn. J. Appl. Phys. **30**, 3700 (1991)
7. C.C. Tsai, Y.J. Lee, J.L. Wang, K.F. Wei, I.C. Lee, C.C. Chen, H.C. Cheng, Solid-State Electron. **52**, 365 (2008)
8. D.H. Auston, C.M. Surko, T.N.C. Venkatesan, R.E. Slusher, J.A. Golovchenko, Appl. Phys. Lett. **33**, 437 (1978)
9. C.C. Kuo, W.C. Yeh, J.F. Lee, J.Y. Jeng, Thin Solid Films **515**, 8094 (2007)
10. C.C. Kuo, W.C. Yeh, J.F. Lee, J.Y. Jeng, Lasers Eng. **17**, 45 (2007)
11. M. He, R. Ishihara, Y. Hiroshima, S. Inoue, T. Shimoda, W. Metselaar, K. Beenakker, Jpn. J. Appl. Phys. **45**, 1 (2006)
12. B. Rezek, C.E. Nebel, M. Stutzmann, Jpn. J. Appl. Phys. **38**, L1083 (1999)
13. C.C. Kuo, W.C. Yeh, C.B. Chen, J.Y. Jeng, Thin Solid Films **515**, 1651 (2006)
14. F.C. Voogt, R. Ishihara, F.D. Tichelaar, J. Appl. Phys. **95**, 2873 (2004)
15. D.H. Lowndes, R.F. Wood, J. Narayan, Phys. Rev. Lett. **52**, 561 (1984)
16. J. Boneberg, P. Leiderer, Phys. Stat. Solids A **166**, 643 (1998)
17. D.H. Auston, C.M. Surko, T.N.C. Venkatesan, R.E. Slusher, J.A. Golovchenko, Appl. Phys. Lett. **33**, 437 (1978)
18. S.R. Stiffler, P. V Evans, A.L. Greer, Acta Metall. Mater. **40**, 1617 (1992)
19. S.J. Park, K.H. Kim, J. Jang, J. Cryst. Grow. **297**, 382 (2006)
20. J.S. Im, M.A. Crowder, R.S. Sposili, J.P. Leonard, H.J. Kim, J.H. Yoon, V.V. Gupta, H.J. Song, H.S. Cho, Phys. Status Solids A **166**, 603 (1998)
21. R. Ishihara, A. Burtsev, P.F.A. Alkemade, Jpn. J. Appl. Phys. **39**, 3872 (2000)
22. L. Mariucci, A. Pecora, G. Fortunato, C. Spinella, C. Bongiorno, Thin Solid Films **427**, 91 (2003)
23. J.S. Im, H.J. Kim, Appl. Phys. Lett. **64**, 2303 (1994)
24. S.R. Stiffler, M.O. Thompson, P.S. Peercy, Phys. Rev. Lett. **60**, 2519 (1988)
25. J.P. Leonard, J.S. Im, Appl. Phys. Lett. **78**, 3454 (2001)
26. V.V. Gupta, H.J. Song, J.S. Im, Appl. Phys. Lett. **71**, 99 (1997)
27. E. Spaepen, D. Turnbull, *Laser Annealing of Semiconductors* (Academic Press, New York, 1982), p. 15
28. L. Mariucci, A. Pecora, R. Carluccio, G. Fortunato, Thin Solid Films **383**, 39 (2001)